processes

Article

Effects of Contact Conditions at Wire–Die Interface on Temperature Distribution during Wire Drawing

Joong-Ki Hwang * and **Young-Chul Chang**

School of Mechatronics Engineering, Korea University of Technology & Education, Cheonan 31253, Republic of Korea
* Correspondence: jkhwang@koreatech.ac.kr; Tel.: +82-41-560-1642

Abstract: The effects of contact conditions at the wire–die interface on the temperature distribution of the specimen and die are investigated to understand the wire drawing process. Finite element analysis and experiments are performed to analyze the temperature distribution of a drawn wire and die based on different contact conditions using a low-carbon steel wire. The maximum temperature (T_{max}) of the die decreases as the contact heat transfer coefficient at the wire–die interface increases, whereas that of the wire increases with the contact heat transfer coefficient. The T_{max} of the die and wire decreases with the thermal conductivity of the die. As the thermal conductivity of the die increases, the heat generated by friction is rapidly absorbed into the die, and the T_{max} of the die decreases, thus resulting in a decrease in the surface temperature of the wire. The T_{max} of both the die and wire linearly increases with the friction factor. In particular, the T_{max} of the die more sensitively changes with the friction factor compared with that of the wire. The T_{max} of the die linearly increases with the drawing velocity, whereas that of the wire parabolically increases with the drawing velocity. The influence of bearing length on the temperature increase in both the wire and die is insignificant.

Keywords: wire drawing; contact conditions; temperature increase; contact heat transfer

Citation: Hwang, J.-K.; Chang, Y.-C. Effects of Contact Conditions at Wire–Die Interface on Temperature Distribution during Wire Drawing. *Processes* **2023**, *11*, 513. https://doi.org/10.3390/pr11020513

Academic Editors: Dariusz Fydrych, Andrzej Kubit, Ankur Gupta, Agnieszka Kowalczyk, Jan Klett, Ján Slota, Wojciech Suder, Balázs Varbai and Abbas Tamadon

Received: 6 January 2023
Revised: 3 February 2023
Accepted: 6 February 2023
Published: 8 February 2023

1. Introduction

Wire drawing is a simple cold metal forming process involving wire, rod, and bar products, such as cables, electrical wires, springs, musical instruments, tire cords, saw wire, wire rope, and so on [1]. During wire drawing, metals show various deformation behaviors depending on the processing temperature because the underlying mechanism of strengthening and ductility of metals is different based on temperature [2–8]. In the wire drawing industries, the temperature increase of both the specimen and die is a significant issue because an excessive increase in temperature during the drawing process deteriorates the product quality, drawability, and die life, particularly in pearlitic steels [9–13]. For example, the temperature increase deteriorated the lubrication property during the process [14], leading to the surface delamination or cracks of the specimen, resulting in the reduction of the drawability of the specimen. In addition, as the strength of the specimen increases with the drawing pass owing to the strain-hardening effect of metals, the deformation resistance of the specimen increases, generating more heat [11]. Furthermore, excessive temperature increase followed by fast cooling sometimes leads to the local surface hardening of the specimen due to the generation of martensite structures. Therefore, the drawing velocity or productivity of the wire, rod, and bar products can increase to a certain extent owing to the temperature rise during wire drawing.

During wire drawing, heat is generated and transferred via several mechanisms, as shown in Figure 1a. The temperature of the specimen is increased by the heat generated by plastic deformation and the heat caused by sliding friction at the wire–die interface. By contrast, the heat of the wire is dissipated via convection and radiation. For example, the heat of the wire is lost to the environment, tools, dies, lubricants, and coolants during wire drawing. The high-pressure contact sliding between the wire and die results in intense conduction heat transfer; therefore, the surface region of the specimen experiences a rapid temperature change during the drawing process. The temperature increase of a drawn wire can be determined by the process conditions, such as the drawing velocity (V_d), reduction in area per pass (R_p), and semi-die angle (α), as well as material properties, such as the thermal conductivity, heat capacity (C_p), density (ρ), strain hardening coefficient (K), and strain hardening exponent (n) of a specimen. In addition, the thermal behavior of the specimen depends on the contact conditions of the wire and die, such as contact heat transfer coefficient (h_c), friction factor between the specimen and die (m), contact length of the wire and die (L_c), bearing length (L_b), and the ratio of thermal conductivity between die (k_d) and wire (k_w) as shown in Figure 1b. The influences of process conditions on the temperature increase of materials have been investigated in recent decades [15–25]. Most of the studies reported that an increase in V_d, R_p, L_b, and m increased the temperature of a specimen. In the case of α, an optimum value of α resulted in a minimal temperature increase.

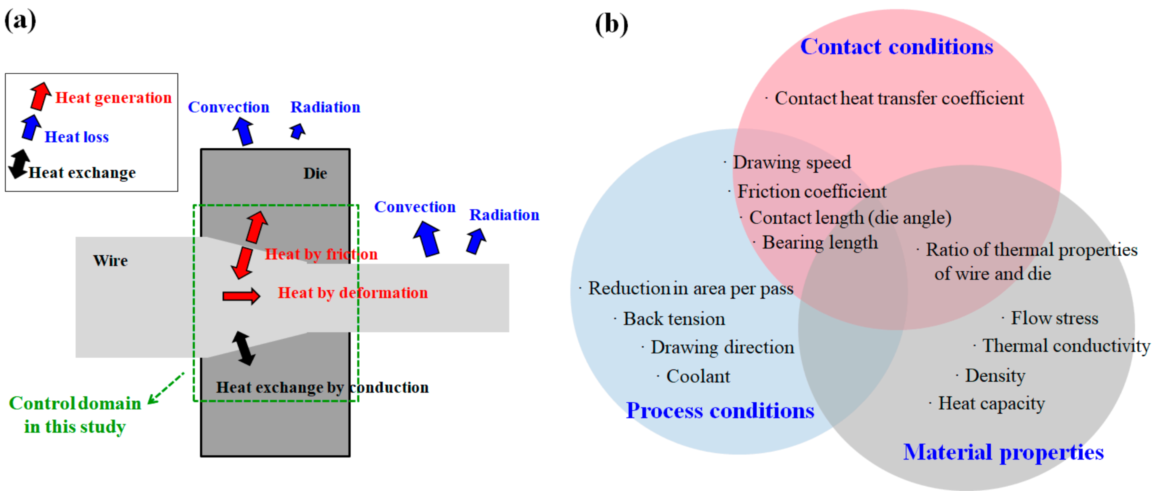

Figure 1. Schematic illustration showing (**a**) heat transfer mechanisms in wire drawing process and (**b**) general parameters affecting temperature distribution of specimen and die during wire drawing.

To the best of the author's knowledge, studies regarding the effects of contact conditions on the temperature increase of a material during wire drawing are insufficient. In particular, studies regarding the effects of contact conditions at the wire–die interface, such as h_c, k_d/k_w, L_c, and L_b on the temperature rise of a specimen are rarely performed. Hence, in this study, the effects of contact conditions on temperature increase are investigated using a low-carbon steel wire to understand the thermal behavior of drawn wire and to improve the wire drawing process from a thermal management standpoint. Finite element analysis (FEA) and experiments are performed to evaluate the temperature increase of deformed specimens and dies based on six contact parameters, i.e., h_c, k_d, L_c, L_b, V_d, and m.

2. Experiment and Numerical Simulation

2.1. Experiment

A low-carbon steel was selected as the test material because this study is primarily interested in the temperature distribution of both the specimen and die depending on the contact conditions rather than the mechanical properties or drawability of the wire with drawing conditions. The low-carbon steel wire rod (13 mm diameter) with a chemical composition of Fe–0.1C–0.4Mn–0.1Si (wt.%) was obtained from POSCO, a steel-making company in Pohang, South Korea. This wire rod steel was fabricated by heating a billet at approximately 1150 °C, performing hot shape rolling at approximately 1000 °C, and conducting air cooling at a cooling rate of 3 °C/s. The microstructure and true stress–strain curve of the hot-rolled wire rod are shown in Figure 2b,c, respectively. The microstructure was characterized via scanning electron microscopy using secondary electrons at 15 kV. To perform a tensile test, the hot-rolled wire rod with a diameter of 13 mm was machined into a tensile specimen with a gage length of 25 mm and a diameter of 5 mm; subsequently, it was strained at a strain rate of 10^{-3} s^{-1} using Instron equipment at 26 °C.

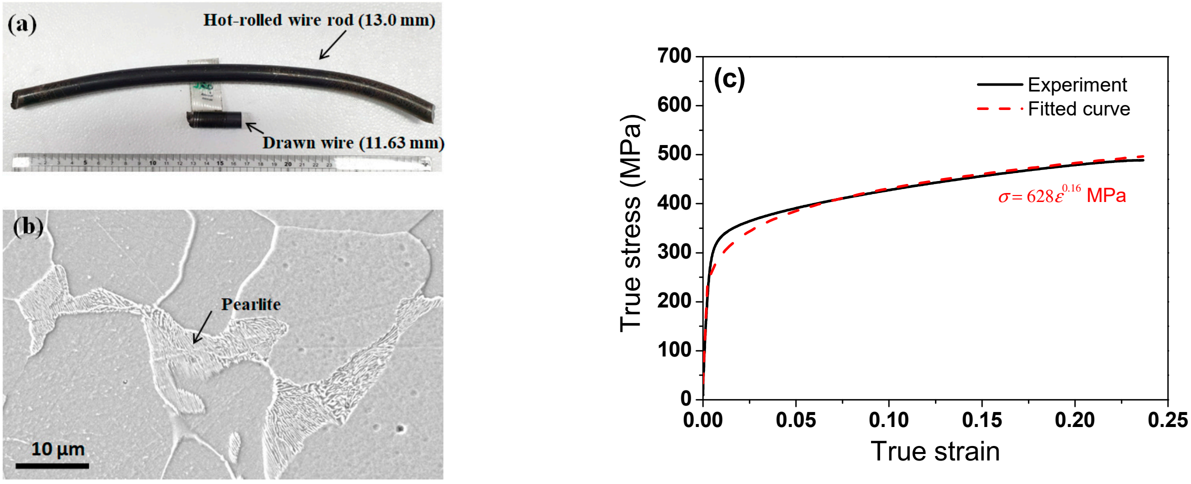

Figure 2. (**a**) Photograph of obtained hot-rolled wire rod steel, (**b**) its microstructure, and (**c**) true stress–strain curve in tensile test.

The wire rod 13 mm in diameter was drawn to a wire measuring 11.63 mm in diameter at a V_d of 0.07 m/s using a single-pass draw bench machine at 26 °C, as shown in Figure 2a. Prior to the drawing, chemical pickling was applied to the wire rod to remove oxidation scales. Subsequently, spray-type molybdenum disulfide (MoS_2) solid lubricant was applied to the specimen owing to its low friction coefficient and good anti-seizure ability originating from the easy cleavage and excellent adhesion to the surface of metals. [26–28]. The α was 6° and the R_p was approximately 20%. The R_p was calculated as follows:

$$R_p = \frac{d_0^2 - d_f^2}{d_0^2} \times 100\ (\%) \quad (1)$$

where d_0 and d_f are the initial and final wire diameters, respectively.

The core temperature of the specimen was measured using a K-type thermocouple measuring 1.0 mm in diameter. To prevent temperature disturbances at the specimen surface, the thermocouple was embedded at the bottom of the wire through a hole measuring 1.0 mm in diameter, as shown in Figure 3 [29]. The drawing force was measured using a load cell installed in the draw bench machine.

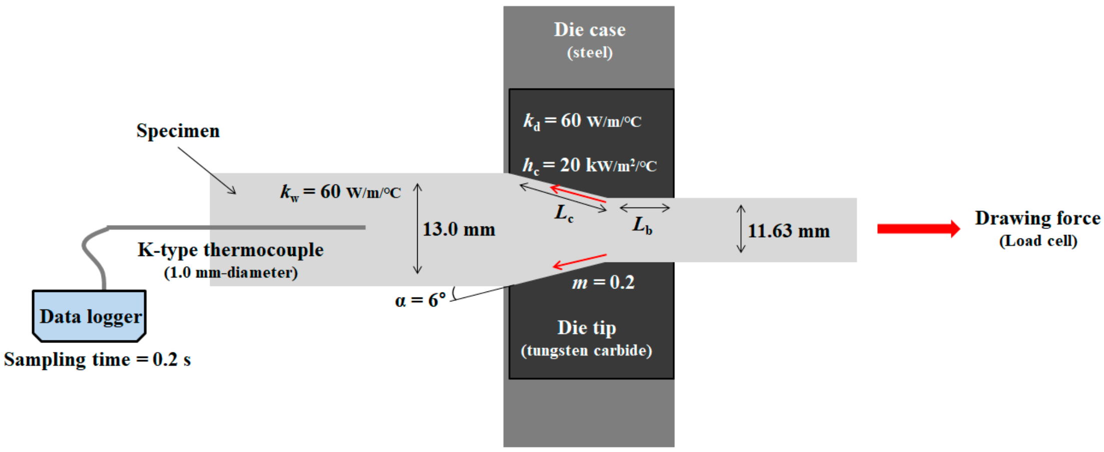

Figure 3. Schematic illustration of wire drawing process performed in this study.

2.2. Finite Element Analysis

During wire drawing, the thermal behavior exhibited by the wire and die is quite complex, as discussed in the Section 1 (Figure 1). To the best of the author's knowledge, it is difficult to measure the surface temperature of rounded small specimens using both radiation-type pyrometers and conduction-type thermocouples [30]. In addition, the surface temperature can be significantly different from that of the inner region of the wire, especially in high-speed wire drawing. For this reason, mathematical models were frequently used to predict the thermal behavior of the wire [12,31]. In this study, FEA was performed to analyze the complex temperature distribution of the specimen with several contact conditions during wire drawing. The DEFORM software (version 11.0, Scientific Forming Technologies Corporation, Columbus, OH, USA was used to simulate the drawing process. The wire rod 13 mm in diameter was drawn to a wire 11.63 mm in diameter. The flow stress curve for the numerical simulation was obtained using the results of the tensile stress–strain curve (Figure 2c). The specimen was considered to be isotropic; therefore, the constitutive behavior of the specimen was described using Hollomon's law, i.e., $\sigma = K\varepsilon^n$. The n and K values of the wire were set as 0.16 and 628 MPa, respectively, by fitting the tensile curve of hot-rolled steel, as shown in Figure 2c. The die was regarded as a rigid body, i.e., the die did not deform during the forming process. L_c is calculated as follows based on Figure 3:

$$L_c = \frac{d_0 - d_f}{2sin\alpha} \tag{2}$$

Friction significantly affects the deformation behavior of a workpiece during plastic forming. In this study, the shear friction model was applied at the die–wire interface owing to the formation of relatively high pressure during wire drawing as follows:

$$\tau = mk \tag{3}$$

where τ is the shear stress on the contact surface and k is the shear yield stress of the material.

The values of m listed in Table 1 were selected to understand the effect of friction on the temperature increase of the specimen and die during wire drawing.

The temperature increase due to plastic deformation was calculated as follows [32,33]:

$$\Delta T_i = \frac{\Delta u}{\rho C_p} = \frac{\beta}{\rho C_p}\int_{\varepsilon_1}^{\varepsilon_2} \sigma d\varepsilon \tag{4}$$

where T_i, Δu, and β are the temperature rise caused by plastic deformation, the generated heat energy, and the fraction factor from mechanical work to heat energy, respectively. β was selected as 0.9 because only a low amount of mechanical work was stored in the deformed wire as elastic energy [32–34]. The thermal properties of the specimen and die, as shown in Figure 3, were assumed to be unaffected by temperature. The following six experimental parameters were selected, and their summary is provided in Table 1:

(i) h_c varied from 1 to 200 kW/m^2/°C.
(ii) k_d varied from 12 to 300 W/m/°C.
(iii) m varied from 0.01 to 0.4.
(iv) V_d varied from 0.05 to 0.3 m/s.
(v) L_c varied from 3.17 to 12.61 mm.
(vi) L_b varied from 1.3 to 7.8 mm.

Table 1. Material properties and process conditions of specimen and die used in FEA. * indicates the standard operating condition.

	Parameter	Wire Rod	Die	Wire–Die Interface
Material properties	Flow stress (MPa)	$\sigma = 628\varepsilon^{0.16}$	Rigid body	-
	Thermal conductivity (k, W/m/°C)	60 [35]	12, 30, 60 *, 120, 300	k_d/k_w of 0.2, 0.5, 1.0 *, 2.0, 5.0
	Specific heat capacity (ρC_p, N/mm^2/°C)	3.6 [32]	3.6	-
	Fraction factor (β)	0.9	-	-
Process conditions	Initial wire diameter (d_o, mm)	13.00	-	-
	Drawn wire diameter (d_f, mm)	-	11.63	-
	Reduction in area per pass (R_p, %)	20	-	-
	Drawing velocity (V_d, m/s)	-	-	0.05, 0.1 0.15 *, 0.3
Contact conditions	Contact length (L_c, mm)	-	3.17, 4.74, 6.31 *, 9.46, 12.61	L_c/d_o of 0.24, 0.36, 0.49 *, 0.73, 0.97
	Bearing length (L_b, mm)	-	1.3, 3.9 *, 7.8	L_b/d_o of 0.1, 0.3 *, 0.6
	Shear friction factor (m)	-	-	0.01, 0.1, 0.2 *, 0.4
	Contact heat transfer coefficient (h_c, kW/m^2/°C)	-	-	1, 5, 10, 20 *, 40, 80, 200

3. Model Validation

Prior to analyzing the temperature distribution of the specimen and die via FEA with the contact conditions, the reliability of the FEA model was verified by comparing the numerically simulated and experimentally measured drawing forces and core temperatures of the low-carbon steel. In this case, m was set as 0.1765 based on a previous study [36]. Owing to the limited ability of the draw bench machine used in this study, the drawing velocity was set to 0.07 m/s. The other operating conditions were identical to standard conditions, as listed in Table 1.

Figure 4 shows a comparison of the drawing forces and core temperatures of the specimen between the experiments and FEA. The simulated drawing force agreed well with the measured value. The prediction error was 1.4%, as listed in Table 2. In terms of temperature, the temperature numerically predicted was slightly higher than that experimentally obtained. The prediction error was 4.0%, which is associated with the friction factor assumed in the FEA. Overall, based on the prediction error for both the drawing force and core temperature, the results of the FEA model are acceptable for further analysis.

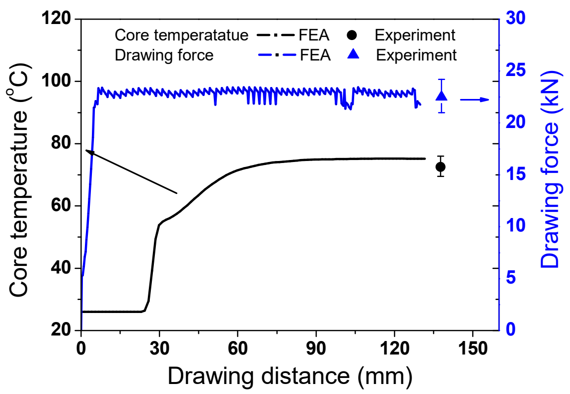

Figure 4. Comparison of core temperature and drawing force between experiment and FEA using low-carbon steel wire rod.

Table 2. Comparison of equilibrium drawing force and core temperature between experiment and FEA.

Parameter	Experiment	FEA	Error (%)
Equilibrium drawing force (kN)	22.5 ± 1.8	22.8 ± 1.4	1.4
Equilibrium core temperature (°C)	72.2 ± 3.7	75.1 ± 0.3	4.0

4. Results and Discussion

4.1. Effect of Contact Heat Transfer Coefficient

During the bulk forming process, h_c is affected by several process parameters, i.e., forming speed, reduction ratio, lubricant, surface roughness of workpiece and tool, tool shape, and specimen temperature. Therefore, researchers have used different values for these parameters to simulate the bulk forming process: the most typically used range for h_c was 5 to 80 kW/m^2/°C [36–42]. For example, Moon et al. [36] determined h_c as 10 kW/m^2/°C for the wire drawing of plain carbon steel. Notably, obtaining the optimum heat transfer coefficient during wire drawing is difficult due to the complexity of deriving h_c and the limitations of the experiments conducted in this study. Hence, the author assumed an appropriate h_c based on the literature review, and then the thermal behaviors of the wire and die were qualitatively compared via FEA.

Figure 5a compares the temperature distribution of the drawn wire calculated via FEA using different values of h_c. The temperatures of both the wire and die varied with h_c. The surface region of the wire exhibited the highest temperature, and the center region of the wire had the lowest temperature during wire drawing. Figure 5b shows the temperature profiles along the radial direction of the drawn wire at the die exit. The wire temperature increased with h_c, particularly at the surface region of the wire. To provide a general overview, Figure 5c shows a summary of the maximum temperature (T_{max}) of the wire and die during the process against h_c. The T_{max} of the die decreased with h_c, whereas that of the wire increased with h_c. The heat caused by friction readily transferred from the die to the wire as h_c increased. From the standpoint of die wear, these results suggest that die wear can be reduced by increasing h_c during wire drawing.

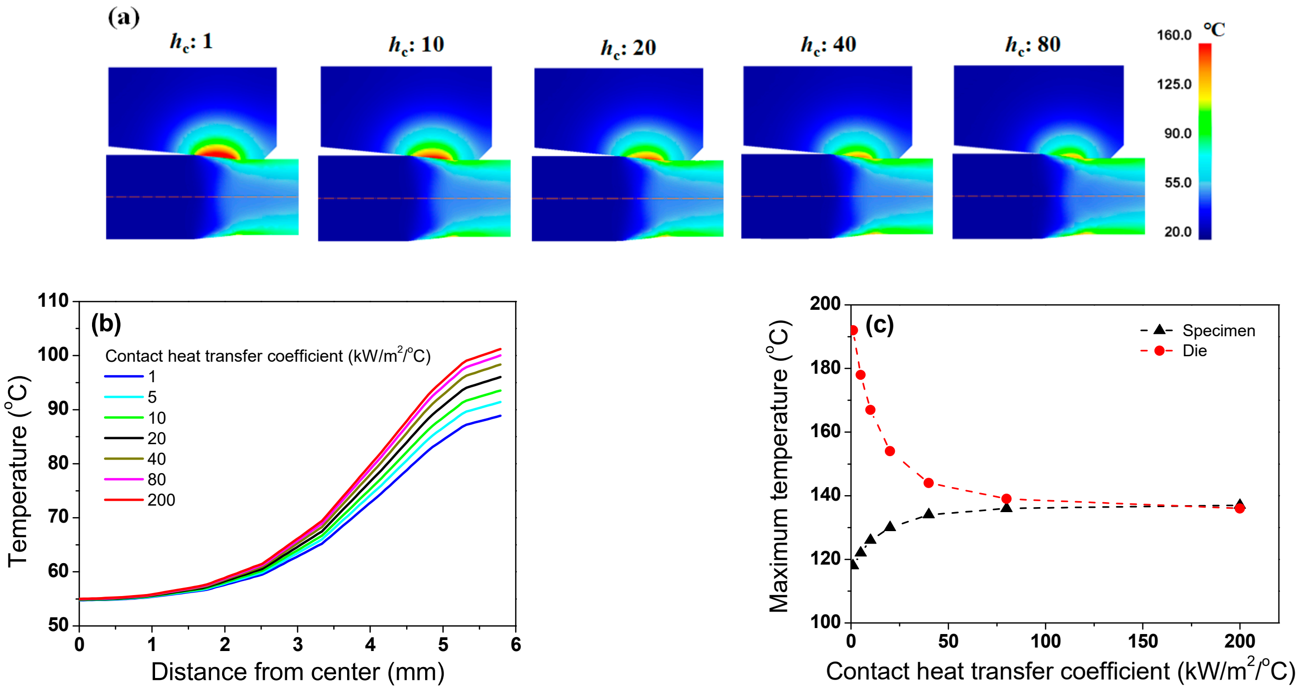

Figure 5. Comparison of temperature (**a**) contours and (**b**) profiles along the radial direction of wire at die exit; (**c**) T_{max} of wire and die vs. contact heat transfer coefficient.

4.2. Effect of Thermal Conductivity of Die

Thermal conductivity is the material's intrinsic ability to conduct heat. Thermal conduction occurs through molecular agitation, not the bulk movement of the solid. Heat moves along a temperature gradient from a high-temperature region to a low-temperature region until thermal equilibrium is reached. Therefore, the heat transfer rate depends on the magnitude of the temperature gradient and the thermal conductivity of the material. For example, Hwang [43] reported that the wire temperature differs with the thermal conductivity of the specimen during wire drawing. The thermal behavior of the specimen and die can differ with the thermal conductivity of the die during wire drawing. Figure 6a shows a comparison of the temperature contours of the drawn wires for different values of k_d. In this study, k_d was normalized by k_w and compared by considering the field applicability. Both the specimen and die temperatures decreased as k_d/k_w increased, which is confirmed by the temperature profiles along the radial direction of the wire at the die exit, as shown in Figure 6b. Figure 6c shows the variation in the T_{max} of the wire and die during the process with k_d/k_w. The T_{max} of the die and wire decreased with increasing k_d/k_w. As k_d increased, the heat generated by friction was rapidly absorbed into the die and the T_{max} of the die decreased. Accordingly, the surface temperature of the wire in the contact region decreased with k_d. In summary, the increase in k_d decreased the die wear as well as the T_{max} of the wire. Meanwhile, the authors believe that it is necessary to study the performance of various drawing dies [44] in view of k_d.

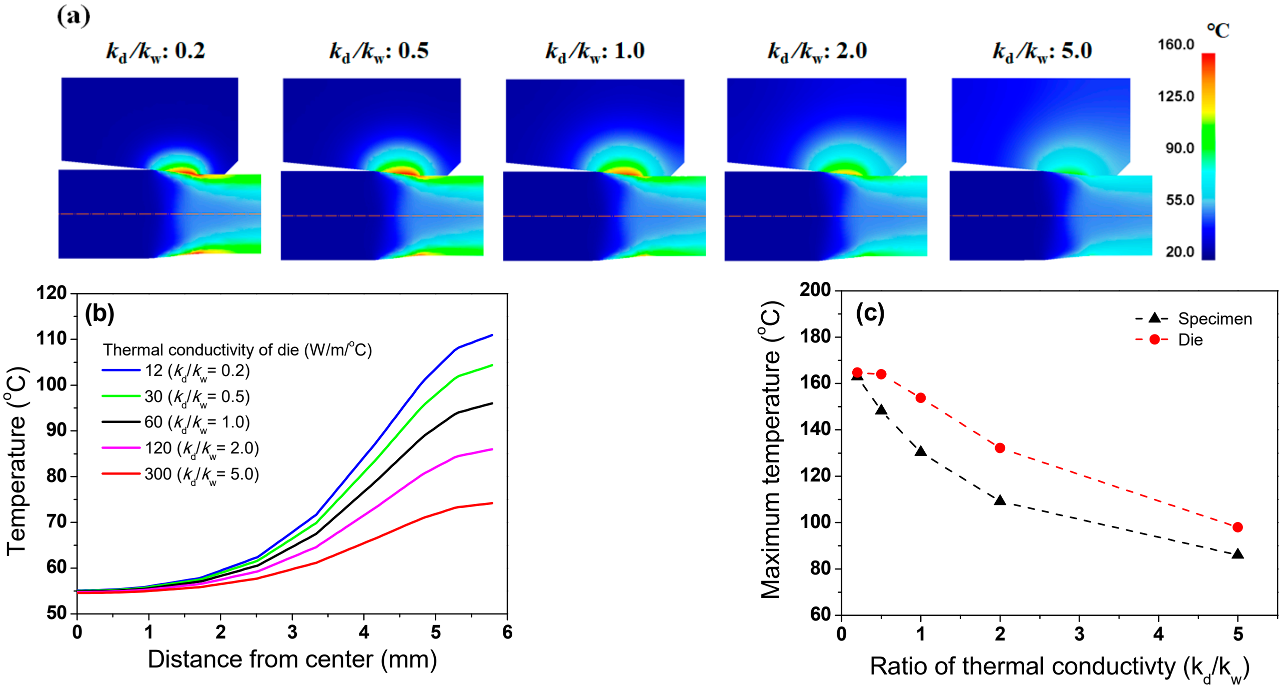

Figure 6. Comparison of temperature (**a**) contours and (**b**) profiles along radial direction of wire at die exit; (**c**) T_{max} of wire and die vs. thermal conductivity of die.

4.3. Effect of Friction

Friction is the non-conservative force resisting the relative motion of the two solid surfaces or fluid layers. When contact surfaces move relative to each other, the frictional force between the two surfaces converts kinetic energy into thermal energy, leading to the temperature increase of the two specimens, particularly the wire and die during wire drawing. Figure 7a shows a comparison of the temperature contours of the wire and die with the different m, and Figure 7b shows the temperature profiles along the radial direction of the wire at the die exit. Although m value varies depending on the contact location between the wire and die due to the different contact pressure with position within the deformation zone [45], a constant value of *m* was assumed in this study regardless of wire position. The temperature gradient along the radial direction of the wire increased with m. The heat caused by friction at the wire–die interface increased with m. Therefore, the temperature in the surface region of the specimen significantly increased with m, which is consistent with the results of previous studies [46,47]. Figure 7c compares the variation in the T_{max} of wire and die during the process against m. The T_{max} of both the die and wire linearly increased with m. In particular, the T_{max} of the die more sensitively changed with m compared with that of the wire.

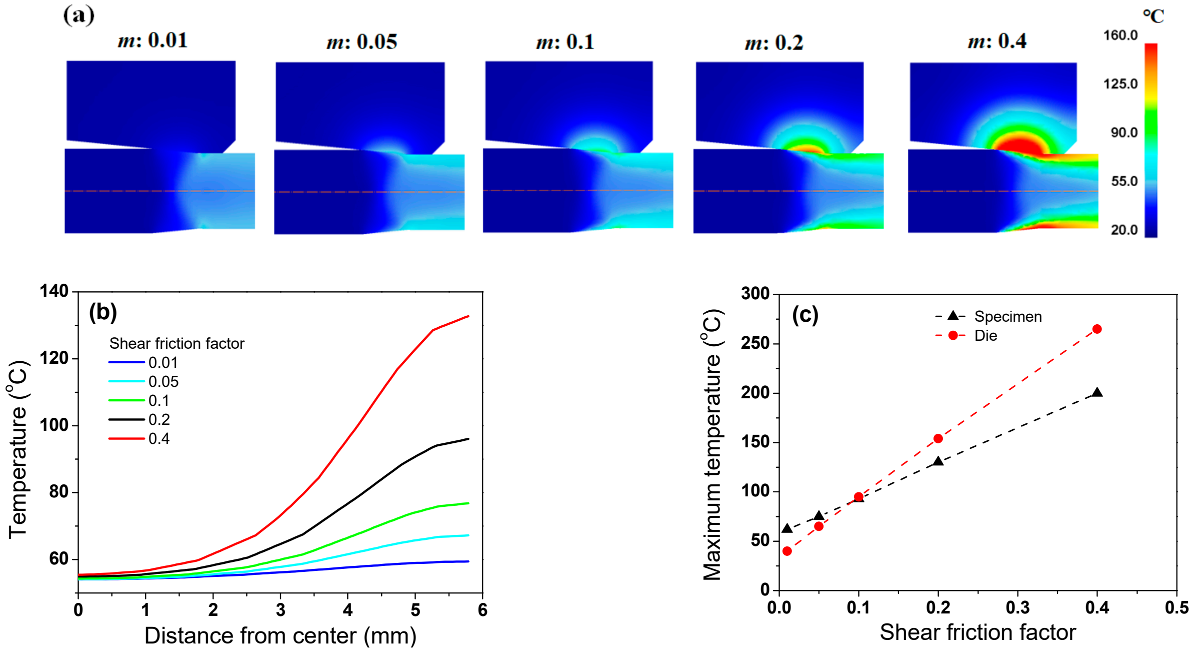

Figure 7. Comparison of temperature (**a**) contours and (**b**) profiles along radial direction of wire at die exit; (**c**) T_{max} of wire and die vs. shear fraction factor.

Meanwhile, it should be noted that the friction coefficient at the wire–die interface and wear of wire typically increased with increasing wire temperature during wire drawing because high temperature softened wire materials and sometimes promoted the oxidation of the metal. The softened materials can be easily sheared and removed under frictional stress, resulting in high wear depth [48]. Therefore, to overcome this drawback, the research on the streamlined die [49,50], hydrodynamic lubrication [51,52], die coating [53], and ultrasonically oscillating dies [54–56] have been conducted in the wire drawing research fields. In addition, the frictional stress at the wire–die interface affected the material properties at the surface of the wire during wire drawing [57].

4.4. Effect of Drawing Velocity

During wire drawing, the wire temperature as well as material properties are significantly affected by V_d [16,18,21,31,58,59]. Figure 8a shows the temperature contours of the specimen and die for the different values of V_d, and Figure 8b shows a comparison of the temperature profiles along the radial direction of the wire at the die exit. As expected, the temperatures of both the wire and die increased with V_d, which is consistent with the previous results [59]. The temperature gradient along the radial direction of the specimen increased with V_d due to the effect of frictional heating. As V_d increased, the temperature gradient inside the wire became stronger because the heat generated by friction at the wire–die interface did not have enough time to be transferred into the wire interior or atmosphere. Meanwhile, the T_{max} of the die linearly increased with V_d, whereas that of the wire parabolically increased with V_d, as shown in Figure 8c. Notably, the temperatures of wire and die can decrease with increasing V_d in view of friction because it is known that the friction coefficient is reduced with increasing V_d in copper wire drawing [60].

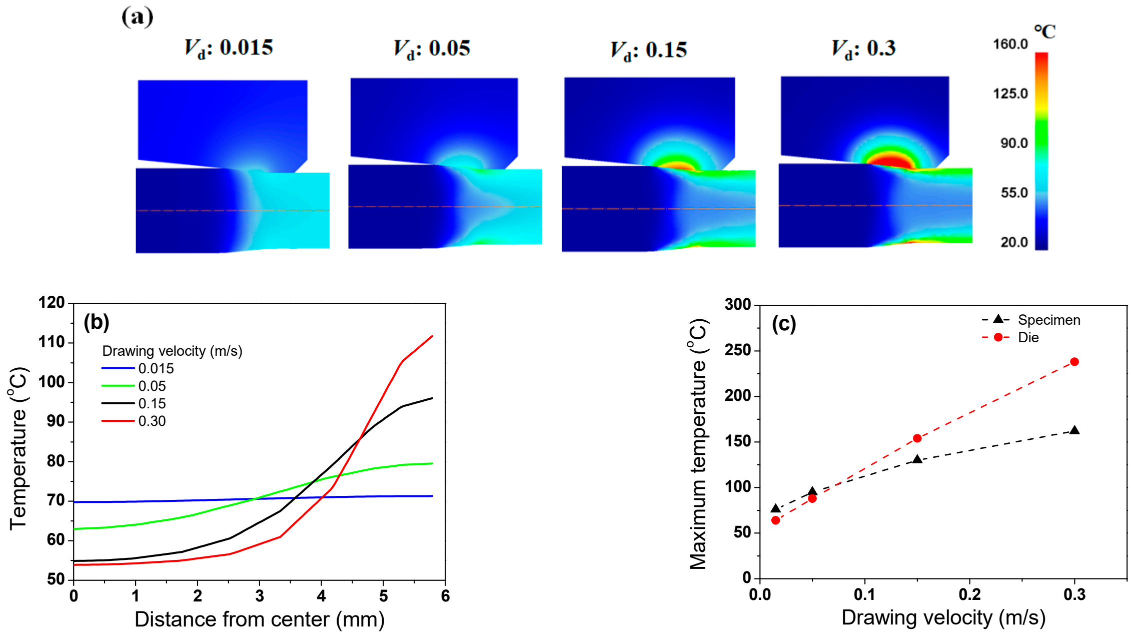

Figure 8. Comparison of temperature (**a**) contours and (**b**) profiles along radial direction of wire at die exit; (**c**) T_{max} of wire and die vs. drawing velocity.

4.5. Effect of Contact Length

The plastic deformation of the specimen takes place within L_c, that is, the deformation zone, and this length was determined by R_p and α during the typical conical die drawing process [61]. Figure 9a compares the temperature contours of the drawn wire and die based on different values of L_c. Both the specimen and die temperatures increased with L_c, as confirmed by the temperature profiles along the radial direction of the wire at the die exit (Figure 9b). Figure 9c shows a comparison of the variation in the T_{max} of wire and die during the process with L_c. The T_{max} of the die and wire increased with L_c owing to the longer wire and die contact time, indicating that the temperatures of wire and die increased with decreasing α in this range of contact conditions during wire drawing.

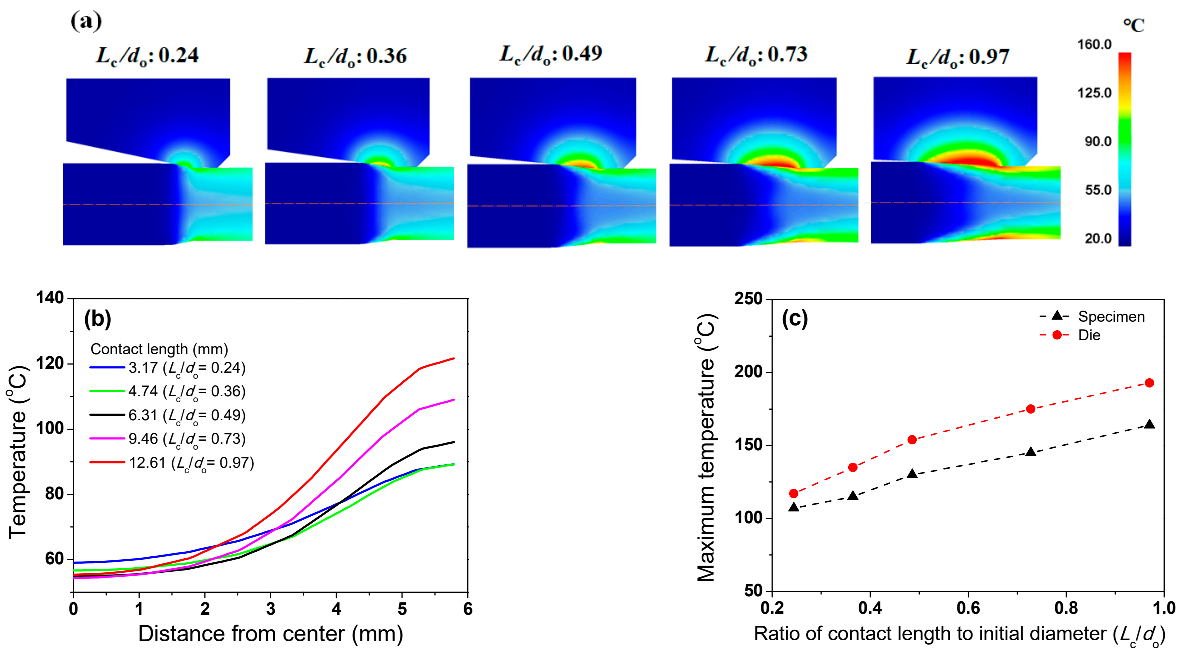

Figure 9. Comparison of temperature (**a**) contours and (**b**) profiles along radial direction of wire at die exit; (**c**) T_{max} of wire and die vs. contact length.

4.6. Effect of Bearing Length

L_b is an important process parameter in the wire drawing process because it determines the final shape and residual stress of the drawn wire [62]. Figure 10a shows the temperature contours of the wire and die for different values of L_b, and Figure 10b shows the temperature profiles along the radial direction of the wire at the die exit. In addition, Figure 10c compares the T_{max} of the die and wire against L_b/d_o. The influence of L_b on the temperature distributions of both the wire and die was insignificant.

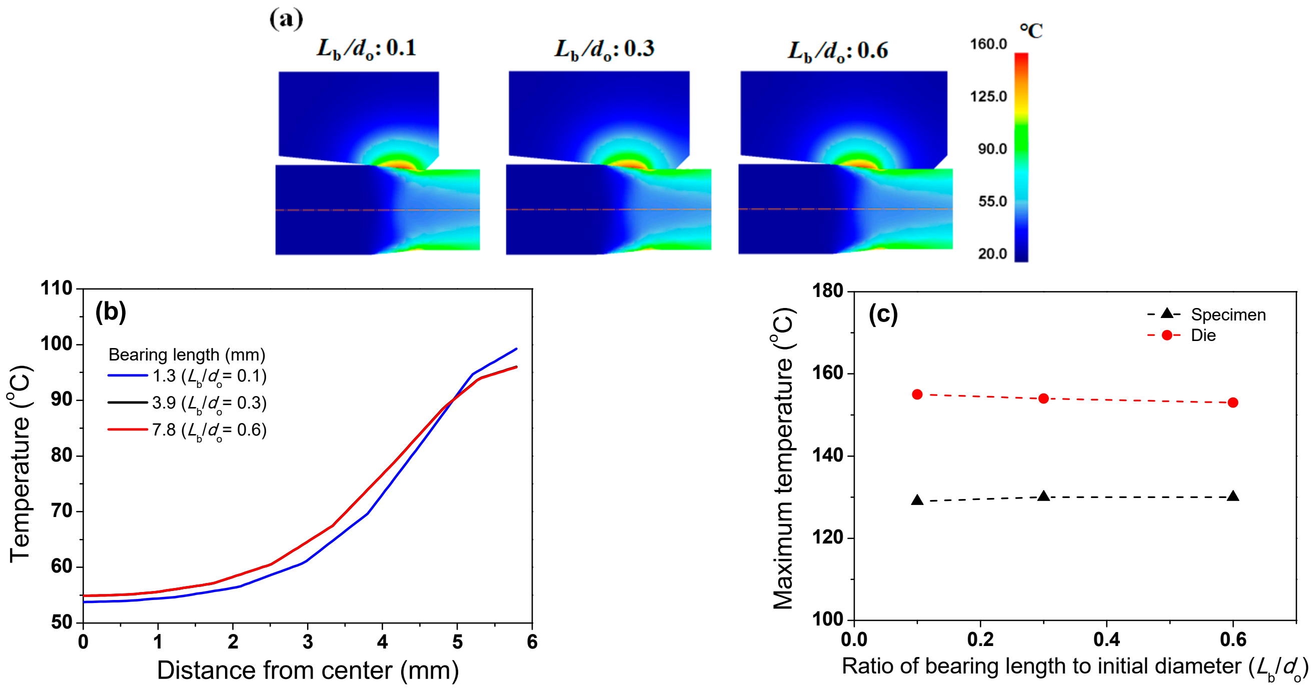

Figure 10. Comparison of temperature (**a**) contours and (**b**) profiles along radial direction of wire at die exit; (**c**) T_{max} of wire and die vs. bearing length.

4.7. Effect of Contact Conditions on Temperature Increase

Figure 11 summarizes the effect of the contact conditions on the temperature increase of the wire and die during wire drawing based on the numerical simulations. The effects of the contact conditions on the temperature distributions of both the wire and die were associated with the heat generated by friction at the wire–die interface. Based on the classical theory of wire drawing [11,63], the total temperature increase of a wire (ΔT_t) comprises temperature rise from ideal plastic deformation (ΔT_i)—as expressed in Equation (4)—temperature increase caused by frictional work (ΔT_f), and temperature increase caused by redundant work (ΔT_r), as follows:

$$\Delta T_t = \Delta T_i + \Delta T_f + \Delta T_r \tag{5}$$

where ΔT_i and ΔT_r depend on R_p, α, n, and K values instead of the contact conditions. The surface temperature of the wire was slightly higher than the central temperature owing to the higher ΔT_r in the surface region originating from the higher effective strain during wire drawing [64,65].

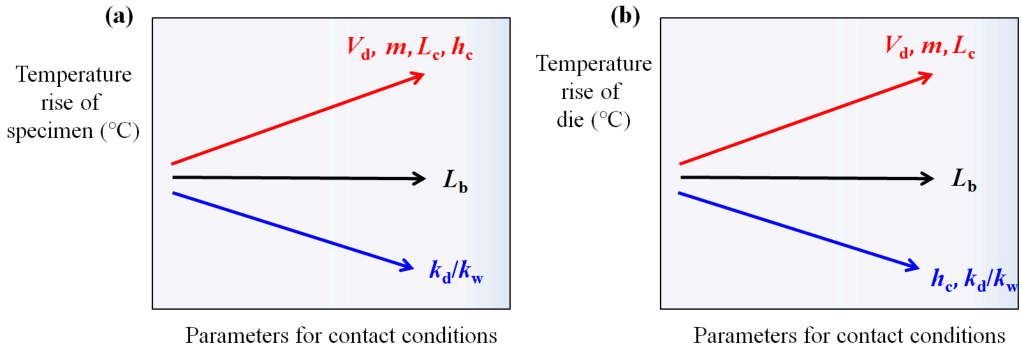

Figure 11. Schematic illustration showing effects of contact conditions on temperature increase in (**a**) specimen and (**b**) die during wire drawing.

By contrast, ΔT_f is significantly affected by the contact conditions during wire drawing. Therefore, the heat generated by friction at the wire–die interface should be prioritized to tailor the temperature distributions of the wire and die. Practically, the die temperature should be decreased during the process to reduce die wear. The die temperature decreased as h_c and k_d increased and V_d, m, and L_c decreased. Therefore, h_c needs to be increased and m should be decreased by selecting the appropriate lubricants and lubrication conditions. In addition, a die material with a high k_d should be used. In the case of wire, h_c, V_d, m, and L_c should be decreased to prevent an increase in temperature of the wire because the temperature rise of the wire deteriorated the performance of lubricants [14], increased the wear of the wire [48], and induced the wire breaks during drawing due to the flow localization originating from the dynamic strain aging effect in plain carbon steels [66]. Notably, the effect of h_c on the temperature increase in the wire and die was different. As h_c increased, the wire temperature increased but the die temperature decreased.

Based on the above results, the engineers in the wire drawing mill should derive optimal process conditions for the drawing process according to the mill situation. Meanwhile, it is necessary to consider that process variables move together. For example, as V_d increases, m decreases [60,67], and the relationship between V_d and m was different with lubricant type and die material [68]. In addition, the V_d and α simultaneously affected the temperature rise of the wire [69], which means that the optimum wire drawing condition varies with V_d depending on the α. The effect of these complex process conditions was not considered in this study.

5. Conclusions

Based on a parametric study of the effects of the contact conditions at the wire–die interface on the temperature distributions of the specimen and die during wire drawing, the following conclusions were obtained:

1. The T_{max} of the die decreased with increasing contact heat transfer coefficient, whereas that of the wire increased with contact heat transfer coefficient. The heat generated by friction at the wire–die interface was readily transferred from the die to the wire with an increasing contact heat transfer coefficient.
2. The T_{max} of the die and wire decreased with increasing thermal conductivity of the die. As the thermal conductivity of the die increased, the heat generated by friction was rapidly absorbed into the die, thus causing the T_{max} of the die to decrease. Accordingly, the surface temperature of the wire at the contact region decreased with the thermal conductivity of the die.
3. The T_{max} of both the die and wire linearly increased with the friction factor. In particular, the T_{max} of the die more sensitively changed with the friction factor compared with that of the wire.

4. The temperature gradient along the radial direction of the wire increased with the drawing velocity because the heat generated by friction at the wire–die interface did not have enough time to be transferred into the wire interior or atmosphere. Meanwhile, the T_{max} of the die linearly increased with drawing velocity, whereas that of the wire parabolically increased with drawing velocity.
5. The T_{max} of the die and wire increased with the contact length of the wire and die owing to the longer wire and die contact time. By contrast, the effect of the bearing length on the temperature increase of both the wire and die was insignificant.

Author Contributions: J.-K.H. designed, wrote, and reviewed the paper and Y.-C.C. performed the data analysis. All authors have read and agreed to the published version of the manuscript.

Funding: This work was supported by the "Education and Research promotion program of KOREATECH in 2022" and "Regional Innovation Strategy (RIS)" through the National Research Foundation of Korea (NRF) funded by the Ministry of Education (MOE)(2021RIS-004).

Data Availability Statement: Not applicable.

Conflicts of Interest: The authors declare no conflict of interest.

Nomenclature

C_p	specific heat (J/kg/K)
d_f	drawn wire diameter (mm)
d_o	initial wire diameter (mm)
h_c	contact heat transfer coefficient (kW/m^2/°C)
K	strain hardening coefficient (MPa)
k	shear yield stress of the material (MPa)
k_d	thermal conductivity of die (W/m/°C)
k_w	thermal conductivity of wire (W/m/°C)
L_b	bearing length (mm)
L_c	contact length (mm)
m	shear friction factor
n	strain hardening exponent
R_p	reduction in area per pass (%)
T	temperature (°C)
ΔT_i	temperature rise from ideal plastic deformation (°C)
ΔT_f	temperature increase caused by frictional work (°C)
ΔT_r	temperature increase caused by redundant work (°C)
ΔT_t	total temperature increase of wire (°C)
V_d	drawing velocity (m/s)
α	semi-die angle (degree)
β	fraction factor between the mechanical work and heat energy
ρ	density (kg/m^3)
τ	shear stress on the contact surface (MPa)

References

1. Newbury, B.D.; Notis, M.R. The history and evolution of wiredrawing techniques. *JOM* **2004**, *56*, 33–37.
2. Strzępek, P.; Mamala, A.; Zasadzińska, M.; Franczak, K.; Jurkiewicz, B. Research on the drawing process of Cu and CuZn wires obtained in the cryogenic conditions. *Cryogenics* **2019**, *100*, 11–17. [CrossRef]
3. Kauffmann, A.; Freudenberger, J.; Klauß, H.; Schillinger, W.; Subramanya Sarma, V.; Schultz, L. Efficiency of the refinement by deformation twinning in wire drawn single phase copper alloys. *Mater. Sci. Eng. A* **2015**, *624*, 71–78.
4. Hwang, J.K. Effect of drawing speed on microstructure distribution and drawability in twinning-induced plasticity steel during wire drawing. *J. Iron Steel Res. Int.* **2020**, *27*, 577–587.
5. Hillery, M.T.; McCabe, V.J. Wire drawing at elevated temperatures using different die materials and lubricants. *J. Mater. Process. Technol.* **1995**, *55*, 53–57.
6. Wei, D.; Min, X.; Hu, X.; Xie, Z.; Fang, F. Microstructure and mechanical properties of cold drawn pearlitic steel wires: Effects of drawing-induced heating. *Mater. Sci. Eng. A* **2020**, *184*, 139341. [CrossRef]

7. Liu, J.P.; Chen, J.X.; Liu, T.W.; Li, C.; Chen, Y.; Dai, L.H. Superior strength-ductility CoCrNi medium-entropy alloy wire. *Scr. Mater.* **2020**, *181*, 19–24.
8. Kubota, H.; Akimoto, Y.; Saito, K.; Sakurazawa, W.; Yoshida, K. Residual Stress Control in Drawn Bar and Wire by Heating-Cooling-Drawing Process. *ISIJ Int.* **2021**, *61*, 2792–2797. [CrossRef]
9. Lee, S.K.; Lee, S.B.; Kim, B.M. Process design of multi-stage wet wire drawing for improving the drawing speed for 0.72 wt% C steel wire. *J. Mater. Process. Technol.* **2010**, *210*, 776–783. [CrossRef]
10. Lee, S.K.; Kim, D.W.; Jeong, M.S.; Kim, B.M. Evolution of axial surface residual stress in 0.82 carbon steel wire during multi pass drawing process considering heat generation. *Mater. Des.* **2012**, *34*, 363–371. [CrossRef]
11. Lee, S.K.; Ko, D.C.; Kim, B.M. Pass schedule of wire drawing process to prevent delamination for high strength steel cord wire. *Mater. Des.* **2009**, *30*, 2919–2927.
12. Jo, H.H.; Lee, S.K.; Kim, M.A.; Kim, B.M. Pass schedule design system in the dry wire-drawing process of high carbon steel. *Proc. IMechE Part B J. Eng. Manuf.* **2002**, *216*, 365–373.
13. Muskalski, Z. Selected problems from the high-carbon steel wire drawing theory and technology. *Arch. Metall. Mater.* **2014**, *59*, 527–535. [CrossRef]
14. Suliga, M. Analysis of the heating of steel wires during high speed multipass drawing process. *Arch. Metall. Mater.* **2014**, *59*, 1475–1480.
15. Hwang, J.K. Fracture behavior of twinning-induced plasticity steel during wire drawing. *J. Mater. Res. Technol.* **2020**, *9*, 4527–4537.
16. Haddi, A.; Imad, A.; Vega, G. Analysis of temperature and speed effects on the drawing stress for improving the wire drawing process. *Mater. Des.* **2011**, *32*, 4310–4315. [CrossRef]
17. Cetinarslan, C.S.; Guzey, A. Tensile properties of cold-drawn low-carbon steel wires under different process parameters. *Mater. Technol.* **2013**, *47*, 245–252.
18. Vega, G.; Haddi, A.; Imad, A. Temperature effects on wire-drawing process: Experimental investigation. *Int. J. Mater. Form.* **2009**, *2*, 229–232. [CrossRef]
19. Suliga, M.; Kruzel, R.; Garstka, T.; Gazdowicz, J. The influence of drawing speed on structure changes in high carbon steel wires. *Metalurgija* **2015**, *54*, 161–164.
20. Pilarczyk, J.W.; Markowski, J.; Dyja, H.; Golis, B. FEM modeling of drawing of wires for prestressed concrete. *Wire J. Int.* **2004**, *37*, 118c123.
21. Nemec, I.; Golis, B.; Pilarczyk, J.W.; Budzik, R.; Waszkielewicz, W. Effect of high-speed drawing on properties of high-carbon steel wires. *Wire J. Int.* **2007**, *40*, 63–68.
22. Rittmann, K. Temperaturerhöhungen der Ziehholoberfläche beim Kaltziehen von Stabstahl mit großen Ziehgeschwindigkeiten. *Arch. Für Das Eisenhüttenwesen* **1971**, *42*, 265–271. [CrossRef]
23. Zhang, G.L.; Wang, Z.W.; Zhang, S.H.; Cheng, M.; Song, H.W. A fast optimization approach for multipass wire drawing processes based on the analytical model. *Proc. IMechE Part B J. Eng. Manuf.* **2013**, *227*, 1023–1031.
24. Strzępek, P.; Mamala, A.; Zasadzińska, M.; Kiesiewicz, G.; Knych, T.A. Shape analysis of the elastic deformation region throughout the axi-symmetric wire drawing process of ETP grade copper. *Materials* **2021**, *14*, 4713.
25. Suliga, M.; Jabłońska, M.; Hawryluk, M. The effect of the length of the drawing die sizing portion on the energy and force parameters of the medium-carbon steel wire drawing process. *Arch. Metall. Mater.* **2019**, *64*, 1353–1359.
26. Farr, J.P.G. Molybdenum disulphide in lubrication. A review. *Wear* **1975**, *35*, 1–22.
27. Vadiraj, A.; Kamaraj, M.; Sreenivasan, V.S. Effect of solid lubricants on friction and wear behaviour of alloyed gray cast iron. *Sadhana* **2012**, *37*, 569–577. [CrossRef]
28. Winer, W.O. Molybdenum disulfide as a lubricant: A review of the fundamental knowledge. *Wear* **1967**, *10*, 422–452.
29. Hwang, J.K. Thermal Behavior of a Rod during Hot Shape Rolling and Its Comparison with a Plate during Flat Rolling. *Processes* **2020**, *8*, 327.
30. Hwang, J.K. Effect of Air Temperature on the Thermal Behavior and Mechanical Properties of Wire Rod Steel during Stelmor Cooling. *ISIJ Int.* **2022**, *62*, 2343–2354.
31. Kemp, I.P.; Pollard, G.; Bramley, A.N. Temperature distributions in the high speed drawing of high strength steel wire. *Int. J. Mech. Sci.* **1985**, *27*, 803–811. [CrossRef]
32. Curtze, S.; Kuokkala, V.T. Dependence of tensile deformation behavior of TWIP steels on stacking fault energy, temperature and strain rate. *Acta Mater.* **2010**, *58*, 5129–5141.
33. Yang, H.K.; Zhang, Z.J.; Dong, F.Y.; Duan, Q.Q.; Zhang, Z.F. Strain rate effects on tensile deformation behaviors for Fe-22Mn-0.6C-(1.5Al) twinning-induced plasticity steel. *Mater. Sci. Eng. A* **2014**, *607*, 551–558.
34. Lee, H.W.; Kwon, H.C.; Im, Y.T.; Hodgson, P.D.; Zahiri, S.H. Local austenite grain size distribution in hot bar rolling of AISI 4135 steel. *ISIJ Int.* **2005**, *45*, 706–712. [CrossRef]
35. Neu, R.W. Performance and characterization of TWIP steels for automotive applications. *Mater. Perform. Charact.* **2013**, *2*, 244–284.
36. Moon, C.; Kim, N. Analysis of wire-drawing process with friction and thermal conditions obtained by inverse engineering. *J. Mech. Sci. Technol.* **2012**, *26*, 2903–2911. [CrossRef]
37. Na, D.H.; Lee, Y. A study to predict the creation of surface defects on material and suppress them in caliber rolling process. *Int. J. Precis. Eng. Manuf.* **2013**, *14*, 1727–1734. [CrossRef]

38. Nalawade, R.S.; Puranik, A.J.; Balachandran, G.; Mahadik, K.N.; Balasubramanian, V. Simulation of hot rolling deformation at intermediate passed and its industrial validity. *Int. J. Mech. Sci.* **2013**, *77*, 8–16.
39. Bagheripoor, M.; Bisadi, H. Effects of rolling parameters on temperature distribution in the hot rolling of alumimum strips. *Appl. Therm. Eng.* **2011**, *31*, 1556–1565. [CrossRef]
40. Wu, J.; Liang, X.; Tang, A.; Pan, F. Interfacial heat transfer under mixed lubrication condition for metal rolling: A theoretical calculation study. *Appl. Therm. Eng.* **2016**, *106*, 1002–1009. [CrossRef]
41. Serajzadeh, S.; Karimi, T.A.; Nejati, M.; Izadi, J.; Fattahi, M. An investigation on strain inhomogeneity in hot strip rolling process. *J. Mater. Process. Technol.* **2002**, *128*, 88–99.
42. Malinowski, Z.; Lenard, J.G.; Davies, M.E. A study of the heat-transfer coefficient as a function of temperature and pressure. *J. Mater. Process. Technol.* **1994**, *41*, 125–142. [CrossRef]
43. Hwang, J.K. Comparison of Temperature Distribution between TWIP and Plain Carbon Steels during Wire Drawing. *Materials* **2022**, *15*, 8696. [CrossRef]
44. Chen, C.; Sun, M.; Wang, B.; Zhou, J.; Jiang, Z. Recent Advances on Drawing Technology of Ultra-Fine Steel Tire Cord and Steel Saw Wire. *Metals* **2021**, *10*, 1590. [CrossRef]
45. Lazzarotto, L.; Dubar, L.; Dubois, A.; Ravassard, P.; Oudin, J. Identification of Coulomb's friction coefficient in real contact conditions applied to a wire drawing process. *Wear* **1997**, *211*, 54–63.
46. Haddi, A.; Imad, A.; Vega, G. The influence of the drawing parameters and temperature rise on the prediction of chevron crack formation in wire drawing. *Int. J. Fract.* **2012**, *176*, 171–180.
47. Radionova, L.V.; Gromov, D.V.; Svistun, A.S.; Lisovskiy, R.A.; Faizov, S.R.; Glebov, L.A.; Zaramenskikh, S.E.; Bykov, V.A.; Erdakov, I.N. Mathematical modeling of heating and strain aging of steel during high-speed wire drawing. *Metals* **2022**, *12*, 1472. [CrossRef]
48. Huang, M.; Fu, Y.; Qiao, X.; Chen, P. Investigation into Friction and Wear Characteristics of 316L Stainless-Steel Wire at High Temperature. *Materials* **2023**, *16*, 213. [CrossRef] [PubMed]
49. Liu, X.Y.; Zhang, S.H. The design of a drawing die based on the logistic function for the energy analysis of drawing force. *Appl. Math. Model.* **2022**, *109*, 833–847.
50. Lo, S.W.; Lu, Y.H. Wire drawing dies with prescribed variations of strain rate. *J. Mater. Process. Technol.* **2002**, *123*, 212–218.
51. Lowrie, J.; Ngaile, G. Analytical modeling of hydrodynamic lubrication in a multiple-reduction drawing die. *J. Manuf. Process* **2017**, *27*, 291–303.
52. Suliga, M.; Wartacz, R.; Hawryluk, M.; Kostrzewa, J. Effect of Drawing in Conventional and Hydrodynamic Dies on Structure and Corrosion Resistance of Hot-Dip Galvanized Zinc Coatings on Medium-Carbon Steel Wire. *Materials* **2022**, *15*, 6728.
53. Nilsson, M.; Olsson, M. Tribological testing of some potential PVD and CVD coatings for steel wire drawing dies. *Wear* **2011**, *273*, 55–59. [CrossRef]
54. Siegert, K.; Möck, A. Wire drawing with ultrasonically oscillating dies. *J. Mater. Process. Technol.* **1996**, *60*, 657–660.
55. Pohlman, R.; Lehfeldt, E. Influence of ultrasonic vibration on metallic friction. *Ultrasonics* **1966**, *4*, 178–185.
56. Liu, S.; Xie, T.; Han, J.; Shan, X. Stress superposition effect in ultrasonic drawing of titanium wires: An experimental study. *Ultrasonics* **2022**, *125*, 106775. [CrossRef]
57. Stolyarov, A.; Polyakova, M.; Atangulova, G.; Alexandrov, S. Effect of die angle and frictional conditions on fine grain layer generation in multipass drawing of high carbon steel wire. *Metals* **2020**, *10*, 1462.
58. Suliga, M.; Wartacz, R.; Michalczyk, J. High speed multi-stage drawing process of hot-dip galvanised steel wires. *Int. J. Adv. Manuf. Technol.* **2022**, *120*, 7639–7655.
59. Wei, D.; Wang, L.; Hu, X.; Mao, X.; Xie, Z.; Fang, F. Effect of drawing strain rate on microstructure and mechanical properties of cold-drawn pearlitic steel wires. *J. Mater. Sci.* **2022**, *57*, 8924–8939. [CrossRef]
60. Santana Martinez, G.A.; Qian, W.L.; Kabayama, L.K.; Prisco, U. Effect of process parameters in copper-wire drawing. *Metals* **2020**, *10*, 105. [CrossRef]
61. Alexandrov, S.; Hwang, Y.M.; Tsui, H.S.R. Determining the Drawing Force in a Wire Drawing Process Considering an Arbitrary Hardening Law. *Processes* **2022**, *10*, 1336.
62. Överstam, H. The influence of bearing geometry on the residual stress state in cold drawn wire, analysed by the FEM. *J. Mater. Process. Technol.* **2006**, *171*, 446–450. [CrossRef]
63. Luis, C.J.; Leon, J.; Luri, R. Comparison between finite element method and analytical methods for studying wire drawing processes. *J. Mater. Process. Technol.* **2005**, *164–165*, 1218–1225. [CrossRef]
64. Luksza, J.; Majta, J.; Burdek, M.; Ruminski, M. Modeling and measurements of mechanical behaviour in multi-pass drawing process. *J. Mater. Process. Technol.* **1998**, *80–81*, 398–405. [CrossRef]
65. Chin, R.K.; Stelf, P.S. A computational study of strain inhomogeneity in wire drawing. *Int. J. Mach. Tools Manuf.* **1995**, *35*, 1087–1098.
66. Karimi Taheri, A.; Maccagno, T.M.; Jonas, J.J. Dynamic Strain Aging and the Wire Drawing of Low Carbon Steel Rods. *ISIJ Int.* **1995**, *35*, 1532–1540.
67. Kabayama, L.K.; Taguchi, S.P.; Martínez, G.A.S. The influence of die geometry on stress distribution by experimental and FEM simulation on electrolytic copper wiredrawing. *Mat. Res.* **2009**, *12*, 281–285. [CrossRef]

68. Martínez, G.A.S.; Rodriguez-Alabanda, O.; Prisco, U.; Tintelecan, M.; Kabayama, L.K. The influences of the variable speed and internal die geometry on the performance of two commercial soluble oils in the drawing process of pure copper fine wire. *Int. J. Adv. Manuf. Technol.* **2022**, *118*, 3749–3760.
69. Prisco, U.; Martinez, G.A.S.; Kabayama, L.K. Effect of die pressure on the lubricating regimes achieved in wire drawing. *Prod. Eng.* **2020**, *14*, 667–676. [CrossRef]